


Cite this: *J. Mater. Chem. A*, 2018, 6, 223

Underoil superhydrophilic desert sand layer for efficient gravity-directed water-in-oil emulsions separation with high flux†

Jian Li, *^{ab} Changcheng Xu,^a Changqing Guo,^a Haifeng Tian,^a Fei Zha^a and Lin Guo*^b

Efficient and rapid separation of emulsified oil/water mixtures is urgently needed and still remains a worldwide challenge. Even though traditional superhydrophobic/superoleophilic filtration membranes have demonstrated to be effective for separation of water-in-oil emulsions, they still suffer from complicated fabrication procedures and lower flux, resulting from their nanoscale pore size. Herein, green desert sands (50 μm to 1 mm) with under-oil superhydrophilicity were introduced, for the first time, to develop into a layer for efficient gravity-directed separation of various water-in-oil emulsions, which could avoid not only sophisticated filtration membranes fabrication process but also the use of expensive low energy materials of fluorosilane involved in traditional superhydrophobic materials. It is worth mentioning that the sand layer could serve as an adsorbent material with under-oil superhydrophilicity, achieving ultrafast gravity-driven separation of tiny water droplets from various water-in-oil emulsions with flux as high as 2342 $\text{L m}^{-2} \text{h}$ even though the interspacing between the sand particles is greater than the size of emulsified droplets. Moreover, the sand can be abundantly obtained from deserts, which is another advantage that the current filtrate materials do not possess. In summary, this study provides a general avenue to design under-oil superhydrophilic materials for rapid separation of water-in-oil emulsions. Such an approach can provide some new perspectives for fabrication of novel emulsion-separating materials.

Received 13th September 2017
Accepted 22nd November 2017

DOI: 10.1039/c7ta08076j

rsc.li/materials-a

1. Introduction

Efficient, rapid and cost-effective processes for the separation of emulsified oil/water mixtures are highly desirable. However, the development of such processes remains a challenge since emulsified oil/water mixtures always exist in multiple forms, such as surfactant-free and surfactant-stabilized emulsions, oil-in-water and water-in-oil emulsions in various environments.^{1,2} Moreover, the emulsified oil/water mixtures often contain numerous droplets with size less than 20 μm , which are more difficult to separate than immiscible oil/water mixtures. In the past decades, several traditional techniques such as oil skimmers, centrifuges, coalescers, magnetic separations and flotation technologies have been implemented for separation of immiscible oil/water mixtures.^{3,4} However, these techniques are not useful for separation of emulsified oil/water mixtures,

making further treatment necessary. Currently, development of filtrate materials with super wettability for efficient separation of emulsified oil/water mixtures, has attracted great attention.^{5–7} In general, these materials are categorized into two types: “water-blocking” and “oil-blocking” materials.⁸ The “water-blocking” materials always exhibit superhydrophobicity/superoleophilicity and filter or adsorb oil from immiscible oil/water mixtures or emulsions. The “oil-blocking” materials always exhibit superhydrophilicity/underwater superoleophilicity and permit water to quickly pass through, while oil is blocked by the water layer trapped in these materials.^{9,10} Until now, various oil-blocking or water-blocking materials have been widely fabricated for efficient separation of various emulsions. The oil-blocking materials such as underwater superoleophobic membranes,^{11–15} porous sponge materials,^{16–19} bi-functional Janus cotton fabric¹⁸ and superhydrophilic foam materials^{20–22} have been commonly used for efficient separation of oil-in-water emulsions. Water-blocking materials, such as superhydrophobic membranes^{23–25} or mesh,^{26–30} superhydrophobic film materials^{31,32} and sponge-like materials with complex micropores, have also been widely used for separation of water-in-oil emulsions.^{33,34} Despite achieving great success in separation of emulsified oil/water mixtures in past years, the drawbacks such as lower flux, greater energy consumption and

^aCollege of Chemistry and Chemical Engineering, Northwest Normal University, Lanzhou 730070, China. E-mail: jianli83@126.com

^bKey Laboratory of Bio-Inspired Smart Interfacial Science and Technology of Ministry of Education, School of Chemistry, BeiHang University, Beijing 100191, P. R. China. E-mail: guolin@buaa.edu.cn

† Electronic supplementary information (ESI) available. See DOI: 10.1039/c7ta08076j

complexity of fabrication processes are major issues that discourage the realization of these materials for large-scale applications. Moreover, the aforementioned drawbacks are essentially resulted from their intrinsic nanoscale pore size. In addition, such smaller pore size is essential for generating the so-called “size-sieving” effect to realize emulsions separation.³⁵ However, the size-sieving separation method is energy consuming as a transmembrane pressure up to several bars is usually required to drive the emulsions to demulsify, and then selectively pass through the membranes.³⁶ Moreover, these materials also suffer from severe decrease in the flux due to surfactant adsorption and/or pore plugging by oil droplets.³⁷ Compared to filtrate materials, the adsorbent materials with high wettability for emulsions disposal possess a unique advantage of avoiding the limitation of smaller nanoscale pore size on flux. To the best of our knowledge, it is still a worldwide challenge for directly adsorbing emulsified droplets from various types of emulsions by the superwetting adsorbent. Recently, a sponge material exhibiting superoleophobicity/superhydrophilicity in air could realize the selective removal of sinking water in oil-rich environments. However, this sponge-like material did not involve adsorption of emulsified water droplets from water-in-oil emulsions.³⁸ In addition, the fabrication process of such materials is rather complicated. Therefore, it is imperative to introduce a facile and low-cost superwetting material to achieve efficient adsorption of emulsified water droplets from various water-in-oil mixtures.

Sand is an inorganic natural resource that is available in abundance in the deserts. In addition, the main component of sand is silicon dioxide.^{39,40} Moreover, sand also contains several metal elements. In general, silicon dioxide and metal particles are covered with a large number of hydroxyl groups, resulting in high surface free energy of these particles. Furthermore, it is their massive hydrophilic compositions with higher surface energy that endows the sand surface with intrinsic water attraction property. Such property of desert sand could be utilized to achieve efficient adsorption of tiny water droplets from various water-in-oil emulsions. To the best of our knowledge, this is the first example of using desert sand for efficient separation of various water-in-oil emulsions with high flux driven solely by gravity. Therefore, the utilization of green, low-cost desert sand to realize efficient separation of various water-in-oil emulsions possesses greater application prospect and laboratory research value.

Herein, we simply cumulated sand particles into a layer, which not only omitted sophisticated film fabrication process but also easily realized the separation of water from water-in-oil emulsions with high flux. The sand layer exhibited excellent underoil superhydrophilicity, which indicated that the sand layer possesses higher water droplets adsorption ability in oil-rich environments. Thus, the sand layer could rapidly capture micron-size water droplets in oil-rich environments to realize both surfactant-stabilized and surfactant-free water-in-oil emulsions separation driven only by gravity, despite the fact that the distance between the sand particles is larger than the size of emulsified droplets. In addition, the separation performances of the sand layer for various water-in-oil emulsions and

their internal mechanisms of emulsion separation were carefully investigated. We firmly believe that such natural desert sand layer is a unique tool to realize large-scale separation of various water-in-oil emulsions.

2. Experimental

2.1. Materials

Sand was directly obtained from the local desert. Mineral water bottles, oils, organic solvents and dyes were purchased from a local store. All the oils and organic solvents were of analytical grade and all aqueous solutions were prepared using distilled water.

2.2. Preparation of sand layer

First, the dirty sands were thoroughly cleaned in distilled water, and then dried in an oven at 90 °C for 2 h. Subsequently, the sands were randomly dropped onto a mesh surface by gravity and finally fixed by another mesh for preventing the loss of sand particles. The diameter of sand layer surface was 1.5 cm. The density (ρ_{layer}) of the sand layer was calculated using the following equation: $\rho_{\text{layer}} = m_{\text{layer}}/V_{\text{layer}}$, where, m_{layer} is the weight of the sand layer, V_{layer} is the volume of the sand layer. The density (ρ_{layer}) of the sand layer was calculated to be 2 g cm⁻³. The porosity (ε) of the sand layer was calculated by the equation: $\varepsilon_{\text{layer}} = \frac{m_{\text{layer}}/\rho_{\text{sand}}}{V_{\text{layer}}} \times 100\%$, where, m_{layer} is the weight of the sand layer, ρ_{sand} is the density of sand ($\rho_{\text{sand}} \approx 2.50$ g cm⁻³), V_{layer} is the volume of the layer; $\varepsilon_{\text{layer}}$ is approximately 79.62%. No other chemical or physical treatments were used prior to the experiments.

2.3. Water-in-oil emulsion separation

The surfactant-stabilized water-in-oil emulsions were prepared by the procedures mentioned below. First, 0.1 g Span 80 was added into four different types of oils (diesel, petroleum ether, kerosene and hexane). Then, water was added dropwise into these oils in a ratio of 1/50 mL/mL with violent agitation. Finally, the mixtures were intensively stirred for more than 6 h until stable milk emulsions were formed. The surfactant-free water-in-oil emulsions without Span 80 were prepared following afore-mentioned procedures. Subsequently, the as-prepared emulsions were poured onto the sand layer and transparent oils were simultaneously collected into a beaker at a constant flux. In addition, the used sand, after simple ethanol treatment, was recycled for further use in the emulsions separation.

2.4. Characterizations

The surface morphology of the sand particles was examined by field emission scanning electron microscopy (FE-SEM). The 3D images of sand were recorded by a non-contact 3D surface contour graph (MicroXAM-800, USA). The contact angles (CAs) were measured using a SL200KB apparatus at ambient temperature, and the volumes of probing liquids in the measurements

were approximately 5 μL . The water content in the collected oil filter was measured using a Karl Fischer Titrator (SN-WS200A). Optical microscopy images were recorded on an inverted fluorescence microscope IX51 (Olympus, Japan) by pouring the emulsions, before and after separation, on a biological counting board. Dynamic light scattering (DLS) measurements were performed on a Zetasizer Nano ZS (Malvern, UK).

3. Results and discussion

Fig. 1 illustrates the preparation process of sand layer and its application in the separation of water-in-oil emulsions. The desert sand was obtained through facial washing, drying procedures, and then, accumulated into a layer onto a stainless steel mesh (300 mesh sizes). Finally, the sand layer was fixed by another identical mesh to prevent the loss of the sand particles. The facile preparation procedure coupled with the low-cost desert sand makes the sand layer a great promise for the large-scale separation of various types of water-in-oil emulsions.

The sand used in our experiments was directly obtained from desert. The surface morphologies of the sand were investigated by FE-SEM. Fig. 2a–c shows the FE-SEM images of sand particles at different magnifications. As shown in Fig. 2a, the sand layer consists of numerous sand particles with different shapes and sizes. Moreover, the large interspaces between the sand particles with diameters greater than 30 μm can also be

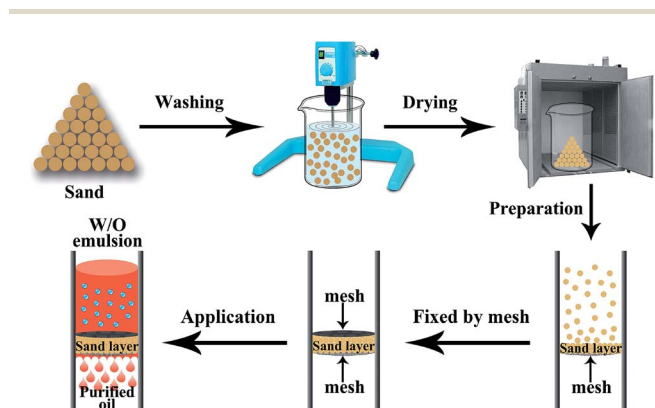


Fig. 1 Illustration of the preparation process of sand layer and its application for the separation of water-in-oil emulsions.

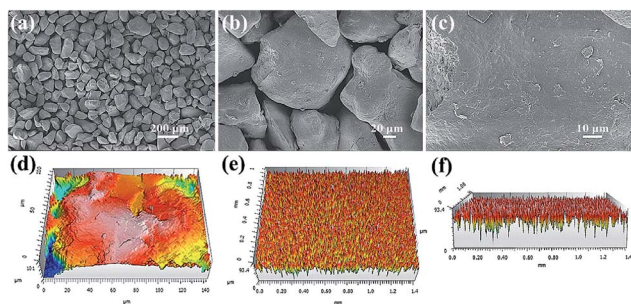


Fig. 2 (a–c) FE-SEM images of sand particles with different magnification. 3D images of (d) sand particle surface and (e, f) sand layer surface.

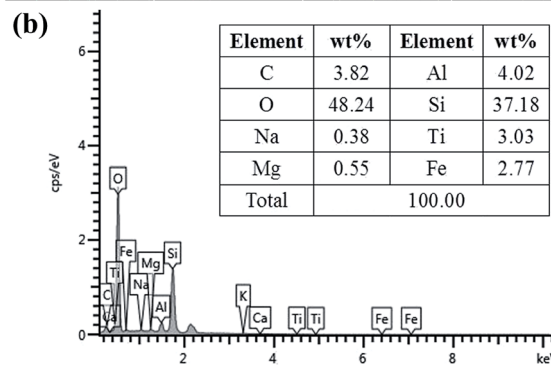
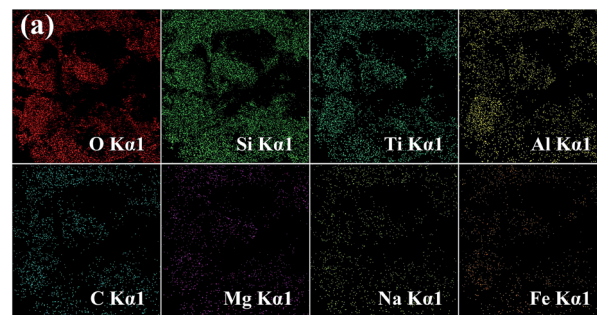


Fig. 3 (a) EDS mapping image of sand. (b) EDS analysis of sand.

observed (Fig. 2b). Moreover, the surface of the sand particles exhibited a micro-sized rough structure instead of smooth surface, and much of the nanoscale debris is randomly distributed over the surface of the sand particles (Fig. 2c). In addition, the topographical texture of the surface of the sand layer was further characterized by 3D surface contour images. As shown in Fig. 2d, the 3D image demonstrated that the sand particle surface possesses an unevenly raised rough structure.^{41,42} Fig. 2e and f shows the 3D images of sand layer surfaces, and the surface roughness was estimated to be approximately dozens of microns. Therefore, the sand layer consists of numerous sand particles with rough surface structure.

The chemical composition of sand was confirmed by energy-dispersive spectrometry (EDS). The EDS mapping images are

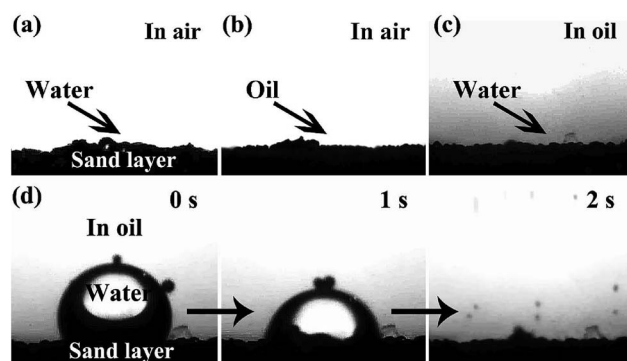


Fig. 4 Wetting behavior of the sand layer towards (a) water in air, (b) oil in air and (c) water in oil. (d) Water contact angle images showing that the water droplet rapidly spreads and wets the sand layer in 2 s, when contacting the sand layer in oil.

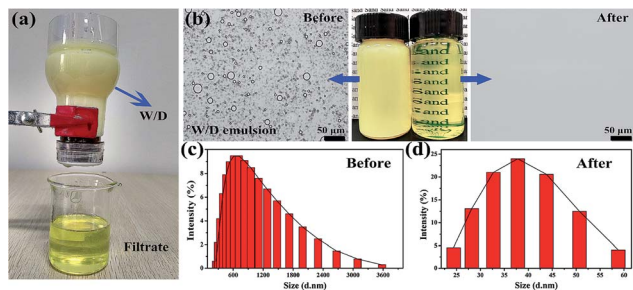


Fig. 5 (a) The setup of separating water-in-diesel emulsion where diesel selectively permeates through the sand layer. (b) Optical microscope images and digital photos, and droplet size distribution of the surfactant-stabilized water-in-diesel (W/D) emulsion (c) before separation (d) after separation.

presented in Fig. 3a. It can be clearly observed that the sand contains many metals. EDS analysis of sand is shown in Fig. 3b, in which two main peaks corresponding to oxygen and silicon can be observed with the atomic percentage of O and Si being 48.24% and 37.18%, respectively. In addition, the other peaks ascribed to C, Na, Mg, Al, Ti and Fe are also presented in Fig. 3b. Moreover, silicon dioxide and metals usually have a high surface free energy. In addition, it is well-known that sand particles contain numerous $-OH$ groups. These results demonstrated that the desert sand possesses numerous chemical compositions with high surface free energy and large number of hydroxyl groups, which endow the sand surface with intrinsic excellent hydrophilic property.

The surface wettability of the sand layer was investigated by a contact angle analyzer. Owing to the high surface free energy and rough surface structure of the sand particles, the sand layer exhibits superhydrophilic and superoleophilic behavior in air as well as under-oil superhydrophilic property. As presented in Fig. 4a and b, when water and oil droplets were dropped onto the sand layer, water was rapidly adsorbed by the sand layer, while the oil droplet quickly spread out on the sand layer; all the obtained contact angle was 0° , indicating superhydrophilicity and superoleophilicity in air. Moreover, the sand layer also exhibited excellent under-oil superhydrophilic behavior. As shown in Fig. 4c, when a water droplet contacted with the sand layer in oil, the water droplet was rapidly caught by sand particles and finally adsorbed by the sand layer (Fig. 4d and Movie S1†), demonstrating under-oil superhydrophilicity. The afore-mentioned special wettability of the sand layer would endow itself superior capture ability toward microsize water droplets in various oil-rich environments.

Due to the superior under-oil superhydrophilicity as well as special surface topography of sand particles, the sand layer could rapidly and efficiently separate various types of water-in-oil emulsions. To evaluate the separation capacity of the sand layer for water-in-oil emulsions, a variety of surfactant-stabilized and surfactant-free water-in-oil emulsions including water-in-diesel, water-in-petroleum ether, water-in-kerosene and water-in-hexane emulsions were prepared. As shown in Fig. 5a, the as-prepared emulsions were poured onto the sand layer to allow the water-in-oil emulsions to be separated (driven only by gravity), which can be clearly seen in Movie S2–S5.†

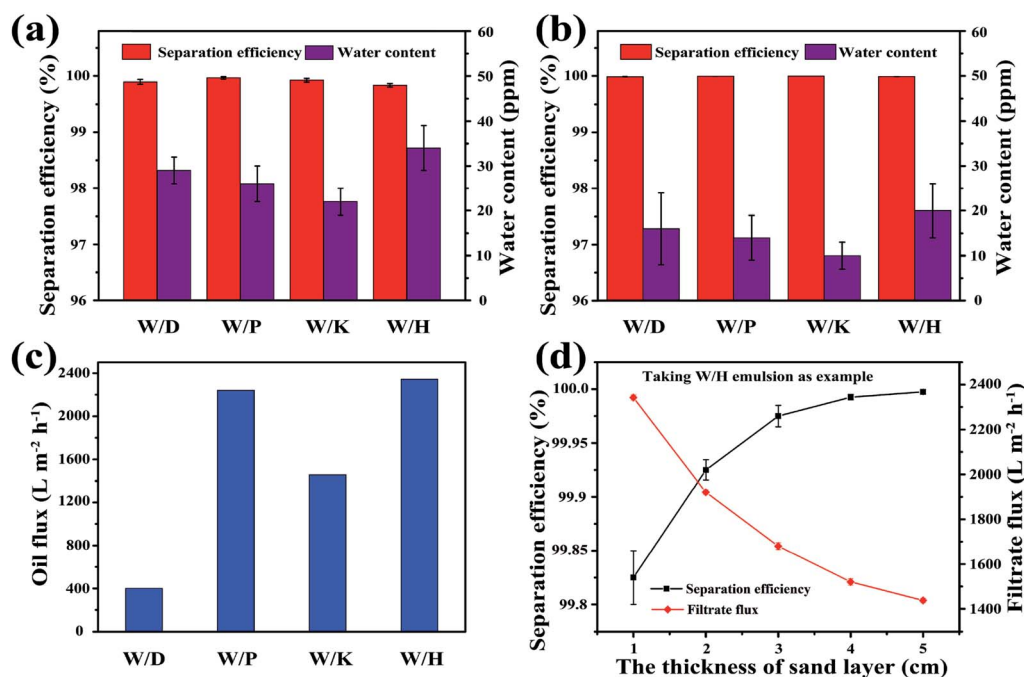


Fig. 6 Separation efficiency and water content in filtrates of (a) surfactant-stabilized and (b) surfactant-free water-in-oil emulsions. (c) Filtrate flux of various surfactant-stabilized water-in-oil emulsions. Condition: the thickness of sand layer is 1 cm, the diameter is 1.0 cm and the volume of separated emulsion is 30 mL. (d) The influence of the thickness of sand layer on separation efficiency and filtrate flux for surfactant-stabilized water-in-hexane emulsion separation.

Table 1 Comparison of the various superwetting filtrate materials for separation of surfactant-stabilized water-in-oil emulsions

Materials	Substrate	Method	Wettability	Driver	Flux	Reference
PVDF membrane	Free standing	Phase inversion method	Superhydrophobicity/ superoleophilicity	0.09 MPa	$1125 \text{ L m}^{-2} \text{ h}^{-1}$	5
SWCNT network film	Free standing	Vacuum filtration method	Hydrophobicity/ superoleophilicity	0.01 MPa	$1587 \text{ L m}^{-2} \text{ h}^{-1}$	32
Polymer/CNTs hybrid membrane	Carbon nanotube	Covalent attachment	Superhydrophobicity/ superoleophilicity	0.01 MPa	$500 \text{ L m}^{-2} \text{ h}^{-1}$	28
SBS-SSM filter	Stainless steel mesh	Electrostatic self-assembling & spin coating method	Superhydrophobicity/ superoleophilicity	Gravity	—	23
CNFs-PDMS inlay-gated SSM	Stainless steel mesh	Vacuum filtration method	Superhydrophobicity/ superoleophilicity	Gravity	$893 \text{ L m}^{-2} \text{ h}^{-1}$	25
PPy-coated SSMs	Stainless steel mesh	Electrochemical polymerization	Superhydrophobicity/ superoleophilicity	Gravity	$350 \text{ L m}^{-2} \text{ h}^{-1}$	26
Polydopamine-silica coated membrane	Stainless steel mesh	Chemistry and Stöber method	Superhydrophobicity/ superoleophilicity	Gravity	—	27
Sand layer	Stainless steel mesh	Stacking method	Underoil superhydrophobicity	Gravity	$2342 \text{ L m}^{-2} \text{ h}^{-1}$	This work

Fig. 5b–d displays the separation results of Span 80 stabilized water-in-diesel (W/D) emulsion. In the digital photos (Fig. 5b), it can be observed that the milky Span 80 stabilized water-in-diesel emulsion turned from opaque (left) to transparent (right) after permeating through the sand layer. Moreover, the optical microscope images of the W/D emulsion before and after separation were captured by an inverted fluorescence microscope. As shown in Fig. 5b, densely packed microsize water droplets are detected in the optical images of original water-in-diesel emulsion, while no water droplets were observed in the entire image of the filtrate, which indicates that all tiny water droplets in the emulsions were successfully removed by the sand layer. In addition, the droplet size distributions of the emulsion before and after separation were measured by dynamic light scattering (DLS). As exhibited in Fig. 5c and d, the water-in-diesel emulsion contained water droplets with a broad size distribution ranging from 255 nm to 3580 nm, which is clearly smaller than the interspace between sand particles that are larger than $20 \mu\text{m}$ (Fig. S1†). In addition, the filtrate exhibited a droplet size distribution ranging from 24.4 nm to 58.8 nm. Moreover, the other Span 80 stabilized water-in-oil emulsions, *i.e.*, water-in-petroleum ether (W/P), water-in-kerosene (W/K) and water-in-hexane (W/H) were also successfully separated and these results can be clearly seen in Fig. S2.† This indicated that the sand layer possesses superior tiny water droplets removal ability from various water-in-oil emulsions.

Furthermore, the separation performances of the sand layer for various water-in-oil emulsions were evaluated by measuring the water content in filtrates and corresponding separation efficiencies. The water content was quantitatively measured by Karl Fischer Titrator. In addition the separation efficiency (R) can be calculated by the equation: $R = 1 - C_f/C_o \times 100\%$, where C_f is the water content in collected filtrate and C_o is the water content in original water-in-oil emulsion. As exhibited in Fig. 6a, the separation efficiency of surfactant-stabilized water-in-oil emulsion is up to 99.98%, while the water content in the corresponding filtrate is less than 34 ppm. Moreover, the separation efficiency of surfactant-free water-in-oil emulsions is up to 99.99% and water content in filtrate is less than 20 ppm (Fig. 6b). Moreover, the sand layer also exhibited higher filtrate flux for various water-in-oil emulsions. As shown in Fig. 6c, the filtrate fluxes for W/D emulsion, W/P emulsion, W/K emulsion and W/H emulsion are all around $400 \text{ L m}^{-2} \text{ h}^{-1}$, $2241 \text{ L m}^{-2} \text{ h}^{-1}$, $1456 \text{ L m}^{-2} \text{ h}^{-1}$ and $2342 \text{ L m}^{-2} \text{ h}^{-1}$, respectively. The above-mentioned filtrate flux was six times larger than that of other filtrate materials directed only by gravity, and still larger than the other filtrate materials driven by external pressure, which are summarized in Table 1. In Fig. 6d, it can be observed that the filtrate flux of water-in-diesel emulsion decreased quasi-exponentially with the increase in the thickness of the sand layer (from 1 cm to 5 cm). In addition, the separation efficiency of water-in-diesel emulsion also increased with increase in the thickness of the sand layer, which was due to a longer effective separation distance (Fig. 6d).

Furthermore, the difference in the flux (J) of various water-in-oil emulsions and the change trend of flux with the thickness of sand layer could be explained by Hagen–Poiseuille equation: $J =$

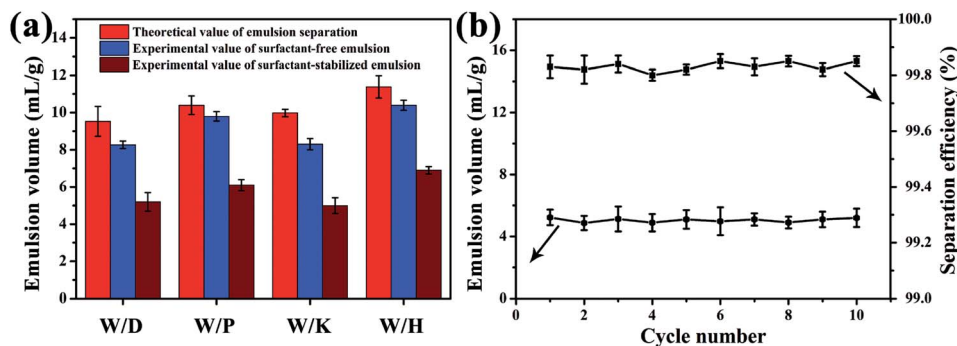


Fig. 7 (a) The theoretical and experimental values of filtrate volumes of both surfactant-free and surfactant-stabilized water-in-oil emulsions separated by the sand layer. (b) Cycling separation performances of the sand layer using surfactant-stabilized water-in-diesel emulsion as an example.

$\varepsilon\pi r_p^2 \Delta p / 8\mu L$, where, ε is the surface porosity, r_p is the pore radius, Δp is the pressure drop, μ is the oil viscosity, and L is the effective filtrate distance.⁴³ Through the analysis of the above formula, we can conclude that the flux is inversely proportional to the viscosity of oils. In addition, the differences in the flux of various emulsions could be observed in Fig. 6c. The flux of W/H and W/P emulsions (5.1 mPa s for diesel, 2.2 mPa s for kerosene) is higher than that of W/D and W/K emulsions (0.3 mPa s for petroleum ether, 0.33 mPa s for hexane). As analyzed above, the filtrate flux of water-in-diesel emulsion is inversely proportional to the effective penetration distance (L). It is worth noting that the water-in-oil emulsions were completely separated only in a single step by simply passing it through the sand layer.

Due to the fact that only a certain amount of water can be adsorbed by the sand layer, the theoretical value (V_g , mL g^{-1}) of separation capacities of various water-in-oil emulsions can be estimated by the equation:

$$V_g = \frac{(m_{\text{saturated}} - m_{\text{wetted}}) / \rho_{\text{water}} \times 50}{m_{\text{raw}}}$$

where, $m_{\text{saturated}}$ is the quality of saturated sand after water adsorption in oil-rich environment, m_{wetted} is the quality of sand after wetted by oil, ρ_{water} is the density of water, m_{raw} is the quality of raw sand and the number 50 is the volume ratio between oil and water in the emulsions. When the sand particles achieve saturated adsorption for water in the process of emulsions separation, the first drop of filtrate turned from transparent to turbid, which indicated the end of separation. As shown in Fig. 7a, the sand layer exhibited higher separation capacities for surfactant-free (above 8 mL g^{-1}) and surfactant-stabilized (above 5 mL g^{-1}) water-in-oil emulsions. The separation capacities of surfactant-stabilized water-in-oil emulsions were lower than that of surfactant-free water-in-oil emulsions, which was ascribed to the fact that tiny water droplets dispersed in surfactant-free emulsions readily coalesce and aggregate into larger droplets than that in surfactant-stabilized emulsions. Moreover, the sand layer also presented superior cycle-usage for surfactant-stabilized water-in-diesel emulsion separation, and the layer exhibited high separation capacity and high separation efficiency even after 10 cycle-usages (Fig. 7b).

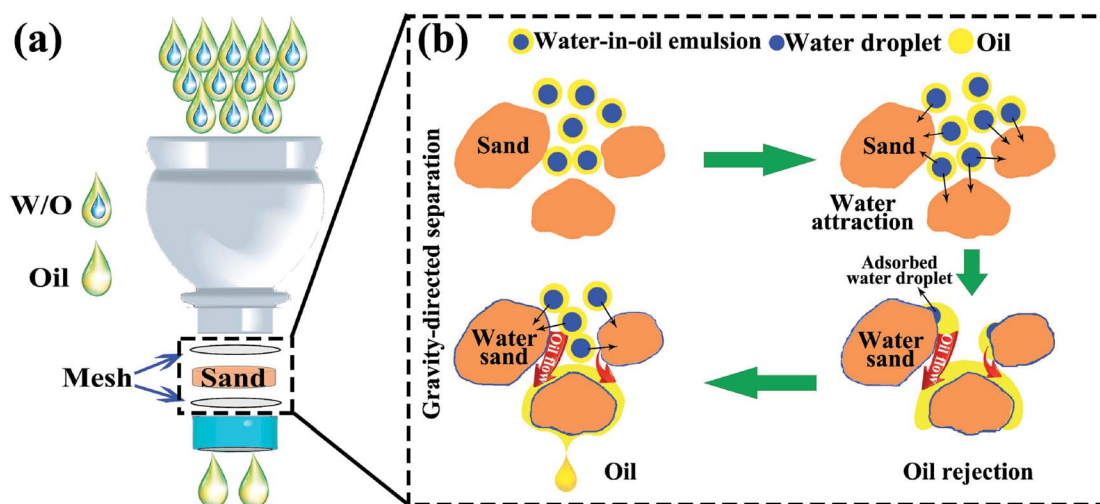


Fig. 8 (a) Schematic illustration of the separation setup, and application of the sand layer for water-in-oil emulsions separation. (b) The procedure for separation of water-in-oil emulsions through the sand layer.

For understanding the separation mechanism of water-in-oil emulsions through the sand layer, the schematic illustration of separation process for water-in-oil emulsions is provided in Fig. 8a. It can be observed that the sand particles were sandwiched between the two meshes in the cap of plastic bottles that act as an adsorption layer, and the as-prepared emulsions were poured onto the sand layer for achieving water-in-oil emulsions separation driven solely by gravity. Moreover, these sand particles in the layer use their selective adsorption ability to harvest tiny water droplets from water-in-oil emulsions. In addition, the details of the separation mechanism of water-in-oil emulsions are illustrated in Fig. 8b. The internal separation mechanism can be depicted as follows: generally, surfaces of high surface energy have stronger affinity to water than oil, while surfaces of low surface energy show stronger affinity to oil.⁴⁴ It is well-known that the main component of sand is silicon dioxide and sand also contains several metal elements. In addition, its chemical composition with high surface energy and hydroxyl groups endow the sand surface with intrinsic water adsorption ability in oil rich environment as shown in Movie S6.† Thus, the surfaces of sand particles possess a tendency to capture water droplets from surfactant-free water-in-oil emulsions. Driven by the high surface energy, the microsize tiny water droplets were easily extracted from the emulsions as soon as the emulsion touches the surfaces of the sand particles. Subsequently, the purified oils continuously passed through the sand layer *via* larger-interspaces between the sand particles. Compared with the surfactant-free water-in-oil emulsion, it is difficult for the surfactant-stabilized tiny water droplets in the emulsions to arrive at the surface of the sand particles, which was due to the fact that tiny water droplets and oil were linked by the hydrophilic and hydrophobic particles of the surfactant, respectively. However, the sand surfaces with high surface energy could provide external surface energy to break such forces, resulting in demulsifying the emulsion droplets; subsequently, the exposed tiny water droplets were captured by the sand particles. Furthermore, the water droplets that covered onto the surfaces of sand particles could induce a higher driving force for further capturing tiny water droplets from the water-in-oil emulsions, resulting in more water droplets to rapidly coalesce and aggregate into massive size droplets around the sand particles surfaces.⁴⁵ Therefore, both surfactant-free and surfactant-stabilized water-in-oil emulsions were separated successfully through the sand particles layer. Exploration of separation mechanism of water-in-oil emulsions on sand particles could be useful in finding novel approaches for ultra-fast gravity-driven separation of various emulsions under the conditions of pore size is greater than that of emulsified droplets.

4. Conclusion

In summary, we have demonstrated the preparation of a green, low-cost desert sand layer through simple washing, drying and stacking procedures. It is worth mentioning that this desert sand layer could serve as an adsorbent material with under-oil superhydrophilicity for efficient gravity-directed separation of various surfactant-stabilized and surfactant-free water-in-oil

emulsions with high flux although the interspaces between sand particles are larger than that of emulsified droplets. In particular, this approach can be easily adapted to other under-oil superhydrophilic inorganic materials for rapidly separation of water-in-oil emulsions. Moreover, the sand layer also showed superior recyclability and high separation efficiency for various water-in-oil emulsions separation. In addition, the sand used in such separations can be directly obtained from desert and does not require any chemical or physical treatments. Therefore, utilization of this facile and green sand layer for the separation of various water-in-oil emulsions would offer a new perspective on practically solving the problems of quality deterioration of fuel caused by activities of humankind.

Conflicts of interest

There are no conflicts to declare.

Acknowledgements

This project was funded by Nature Science Foundation of China (21301141), China Postdoctoral Science Foundation (2017M610031), the Yong Teacher Research Group Foundation of Northwest Normal University (NWNLU-LKQN-16-6) and the Guangdong Provincial Key laboratory of New and Renewable Energy Research and Development (No. Y707sc1001).

Notes and references

- 1 T. Mason, J. Wilking, K. Meleson, C. Chang and S. Graves, *J. Phys.: Condens. Matter*, 2006, **18**, R635.
- 2 B. Wang, W. Liang, Z. Guo and W. Liu, *Chem. Soc. Rev.*, 2015, **44**, 336–361.
- 3 G. Kwon, A. Kota, Y. Li, A. Sohani, J. Mabry and A. Tuteja, *Adv. Mater.*, 2012, **24**, 3666–3671.
- 4 M. Cheryan and N. Rajagopalan, *J. Membr. Sci.*, 1998, **151**, 13–28.
- 5 W. Zhang, Z. Shi, F. Zhang, X. Liu, J. Jin and L. Jiang, *Adv. Mater.*, 2013, **25**, 2071–2076.
- 6 M. Tao, L. Xue, F. Liu and L. Jiang, *Adv. Mater.*, 2014, **26**, 2943–2948.
- 7 J. Fan, Y. Song, S. Wang, J. Meng, G. Yang, X. Guo, L. Feng and L. Jiang, *Adv. Funct. Mater.*, 2015, **25**, 5368–5375.
- 8 W. Zhang, N. Liu, Y. Cao, X. Lin, Y. Liu and L. Feng, *Adv. Mater. Interfaces*, 2017, **4**, 1700029.
- 9 J. Li, D. Li, Y. Yang, J. Li, F. Zha and Z. Lei, *Green Chem.*, 2016, **18**, 541–549.
- 10 J. Li, Z. Zhao, D. Li, H. Tian, F. Zha, H. Feng and L. Guo, *Nanoscale*, 2017, **9**, 13610–13617.
- 11 T. Yuan, J. Meng, T. Hao, Z. Wang and Y. Zhang, *ACS Appl. Mater. Interfaces*, 2015, **7**, 14896–14904.
- 12 W. Zhang, Y. Zhu, X. Liu, D. Wang, J. Li, L. Jiang and J. Jin, *Angew. Chem., Int. Ed.*, 2014, **53**, 856–860.
- 13 Z. Wang, X. Jiang, X. Cheng, C. Lau and L. Shao, *ACS Appl. Mater. Interfaces*, 2015, **7**, 534–9545.
- 14 J. Ge, J. Zhang, F. Wang, Z. Li, J. Yu and B. Ding, *J. Mater. Chem. A*, 2017, **5**, 497–502.

- 15 L. Zhang, J. Gu, L. Song, L. Chen, Y. Huang and J. Zhang, *J. Mater. Chem. A*, 2016, **4**, 10810–10815.
- 16 G. Wang, Y. He, H. Wang, L. Zhang, Q. Y. Yu, S. Peng, X. Wu, T. Ren, Z. Zeng and Q. Xue, *Green Chem.*, 2015, **17**, 3093–3099.
- 17 J. Li, C. Xu, Y. Zhang, R. Wang, F. Zha and H. She, *J. Mater. Chem. A*, 2016, **4**, 15546–15553.
- 18 L. Xu, Y. Chen, N. Liu, W. Zhang, Y. Yang, Y. Cao, X. Lin, Y. Wei and L. Feng, *ACS Appl. Mater. Interfaces*, 2015, **7**, 22264–22271.
- 19 M. Khosravi and S. Azizian, *ACS Appl. Mater. Interfaces*, 2015, **7**, 25326–25333.
- 20 Z. Wang, Y. Wang and G. Liu, *Angew. Chem., Int. Ed.*, 2015, **54**, 1–5.
- 21 Z. Luo, S. Lyu, Y. Wang and D. Mo, *Ind. Eng. Chem. Res.*, 2017, **56**, 699–707.
- 22 Y. Zhang, X. Yang, Z. Wang, J. Long and L. Shao, *J. Mater. Chem. A*, 2017, **5**, 7316–7325.
- 23 J. Gu, P. Xiao, Y. Huang, J. Zhang and T. Chen, *J. Mater. Chem. A*, 2015, **3**, 4124–4128.
- 24 X. Lin, M. Choi, J. Heo, H. Jeong, S. Park and J. Hong, *ACS Sustainable Chem. Eng.*, 2017, **5**, 3448–3455.
- 25 Y. Li, Z. Zhang, M. Wang, X. Men and Q. Xue, *J. Mater. Chem. A*, 2017, **5**, 5077–5087.
- 26 Z. Wang, C. Xiao, Z. Wu, Y. Wang, X. Du, W. Kong, D. Pan, G. Guan and X. Hao, *J. Mater. Chem. A*, 2017, **5**, 5895–5904.
- 27 Y. Cai, D. Chen, N. Li, Q. Xu, H. Li, J. He and J. Lu, *J. Mater. Chem. A*, 2016, **4**, 18815–18821.
- 28 X. Lin, J. Heo, H. Jeong, M. Choi, M. Chang and J. Hong, *J. Mater. Chem. A*, 2016, **4**, 17970–17980.
- 29 M. Liu, Y. Hou, J. Li and Z. Guo, *Langmuir*, 2017, **33**, 3702–3710.
- 30 Y. Cao, Y. Chen, N. Liu, X. Lin, L. Feng and Y. Wei, *J. Mater. Chem. A*, 2014, **2**, 20439–20443.
- 31 J. Gu, P. Xiao, J. Chen, F. Liu, Y. Huang, G. Li, J. Zhang and T. Chen, *J. Mater. Chem. A*, 2014, **2**, 15268–15272.
- 32 W. Zhang, N. Liu, Y. Cao, Y. Chen, L. Xu, X. Lin and L. Feng, *Adv. Mater.*, 2015, **27**, 7349–7355.
- 33 J. Yun, F. Khan and S. Baik, *ACS Appl. Mater. Interfaces*, 2017, **9**, 16694–16703.
- 34 Y. Si, Q. Fu, X. Wang, J. Zhu, J. Yu, G. Sun and B. Ding, *ACS Nano*, 2015, **9**, 3791–3799.
- 35 Z. Shi, W. Zhang, F. Zhang, X. Liu, D. Wang, J. Jin and L. Jiang, *Adv. Mater.*, 2013, **25**, 2422–2427.
- 36 W. Zhang, Y. Zhu, X. Liu, D. Wang, J. Li, L. Jiang and J. Jin, *Angew. Chem., Int. Ed.*, 2014, **53**, 856–860.
- 37 B. Al-anzi and O. Siang, *RSC Adv.*, 2017, **7**, 20981–20994.
- 38 Z. Xu, Y. Zhao, H. Wang, X. Wang and T. Lin, *Angew. Chem., Int. Ed.*, 2015, **54**, 4527–4530.
- 39 J. Yong, F. Chen, Q. Yang, H. Bian, G. Du, C. Shan, J. Huo, Y. Fang and X. Hou, *Adv. Mater. Interfaces*, 2016, **3**, 1500650–1500656.
- 40 L. Chen, Y. Si, Z. Guo and W. Liu, *J. Mater. Chem. A*, 2017, **5**, 6416–6423.
- 41 T. Norgaard and M. Dacke, *Front. Zool.*, 2010, **7**, 23.
- 42 A. Parker and C. Lawrence, *Nature*, 2001, **414**, 33–34.
- 43 X. Peng, J. Jin, Y. Nakamura, T. Ohno and I. Ichinose, *Nat. Nanotechnol.*, 2009, **4**, 353–357.
- 44 G. Liu, M. Cai, X. Wang, F. Zhou and W. Liu, *ACS Appl. Mater. Interfaces*, 2014, **6**, 11625–11632.
- 45 X. Zeng, L. Qian, X. Yuan, C. Zhou, Z. Li, J. Cheng, S. Xu, S. Wang, P. Pi and X. Wen, *ACS Nano*, 2017, **11**, 760–769.